Journal of Guidance, Control, and Dynamics, Vol. 42, No. 2, 2019, pp. 425–431. doi: http://doi.org/10.2514/1.G003788

Stability and Control of Spinning Electric Solar Wind Sail in Heliostationary Orbit

Marco Bassetto*, Giovanni Mengali,† and Alessandro A. Quarta‡
Department of Civil and Industrial Engineering, University of Pisa, I-56122 Pisa, Italy

Nomenclature

$\mathbb{A}$	=	state matrix, see Eq. (43)
b	=	reference length, see Eq. (11)
f	=	distance of dx from (x_B, y_B) plane, m
$\boldsymbol{F}$	=	thrust vector, with $\|\|\boldsymbol{F}\|\| \triangleq F$, N
F_x, F_y, F_z	=	components of $\boldsymbol{F}$ in $\mathcal{T}_I$, N
g	=	auxiliary function, see Eqs. (49)
h	=	dimensionless parameter, see Eq. (41)
I_t, I_z	=	transverse and longitudinal moments of inertia, kg m^2
$\hat{\boldsymbol{\imath}}$, $\hat{\boldsymbol{\jmath}}$, $\hat{\boldsymbol{k}}$	=	unit vectors of $\mathcal{T}_B$
$\hat{\boldsymbol{\imath}}_I$, $\hat{\boldsymbol{\jmath}}_I$, $\hat{\boldsymbol{k}}_I$	=	unit vectors of $\mathcal{T}_I$
k	=	gain
k_x, k_y, k_z	=	components of $\hat{\boldsymbol{k}}$ in $\mathcal{T}_I$
L	=	tether length, m
$\mathcal{M}$	=	shape coefficient, see Eq. (6)
m	=	spacecraft mass, kg
m_p	=	proton mass, kg
n	=	solar wind number density, m^{-3}
N	=	number of tethers
$\mathcal{P}$	=	shape coefficient, see Eq. (5)
q_1, q_2	=	state variables, see Appendix
$\hat{\boldsymbol{r}}$	=	sun-spacecraft unit vector
r	=	sun-spacecraft distance, m
S	=	spacecraft center-of-mass
$\boldsymbol{T}$	=	torque vector, N m
t	=	time, s
u	=	solar wind speed, m/s
$\mathscr{V}$	=	Lyapunov function, see Eq. (51)
V	=	tether electric potential, V
V_w	=	solar wind electric potential, V
x	=	curvilinear abscissa, m
$\boldsymbol{x}$	=	dimensionless state vector, see Eq. (43)
x_B, y_B, z_B	=	axes of $\mathcal{T}_B$
x_I, y_I, z_I	=	axes of $\mathcal{T}_I$
α_n	=	pitch angle, rad
δ_n	=	clock angle, rad
ϵ_0	=	vacuum permittivity, F/m
ζ	=	damping factor
θ, ϕ, ψ	=	Euler's angles, rad
λ	=	Smelt's parameter
$\mu_\odot$	=	sun's gravitational parameter, m^3/s^2
ν	=	dimensionless radial error
ρ	=	tether linear mass density, kg/m
σ	=	design parameter, see Eq. (4), kg/m/s
τ	=	tether tension force, N
$\mathcal{T}_B$	=	body reference frame
$\mathcal{T}_I$	=	inertial reference frame
$\boldsymbol{\Omega}$	=	spacecraft angular velocity vector, rad/s
ω_n	=	natural frequency, rad/s
Ω_x, Ω_y, ω	=	components of spacecraft angular velocity in $\mathcal{T}_B$, rad/s

Subscripts

d	=	derivative
max	=	maximum
min	=	minimum
p	=	proportional
t	=	tip
0	=	initial
$\oplus$	=	at 1 au from the sun

*Ph.D. student, marco.bassetto@ing.unipi.it
†Professor, g.mengali@ing.unipi.it. Senior Member AIAA.
‡Professor, a.quarta@ing.unipi.it. Associate Fellow AIAA (**corresponding author**).

Superscripts

$'$	=	derivative with respect to x
$\cdot$	=	time derivative
$-$	=	nominal
$\sim$	=	dimensionless

Introduction

High-energy missions or complex spacecraft trajectories that would be very difficult (or even impossible) to obtain with conventional thrusters, may become feasible with the use of a propellantless propulsion system, such as a solar sail or an Electric Solar Wind Sail (E-sail) [1, 2]. In particular, the latter generates thrust by exchanging momentum with solar wind particles [1]. The incoming ions from the sun interact with an artificial electric field produced by means of long charged tethers, which are kept at a high voltage level, on the order of few tens of kilovolts [3]. The spacecraft is spun around a symmetry axis to deploy the tethers and maintain them stretched, so as to resemble, in an ideal case, a rigid disc [4, 5].
The use of a propellantless system that provides a continuous thrust, capable of being modulated within some limits, is a fundamental requirement for tracking non-Keplerian orbits [6–9], generating artificial Lagrange points [10,11], or maintaining a heliostationary condition [12–14]. In the latter case, the spacecraft is first required to reach a point in the interplanetary space with zero absolute velocity [12,14], and then to exploit its propulsive acceleration for balancing the solar gravitational attraction and maintaining such a still condition relative to an inertial (heliocentric) reference frame. Possible scientific missions for a heliostationary spacecraft [13] include the sun's observation, the monitoring for near-Earth objects, or the release of a small solar probe along a rectilinear trajectory [15, 16]. Since a heliostationary condition requires a high-performance propulsion system, which is beyond the current technology level for both solar sails [17] and E-sails [4], such an advanced mission scenario can be considered as a technological challenge for a propellantless thruster [18].

The problem of maintaining a heliostationary position is especially involved, from a control point of view, for an E-sail-based spacecraft whose propulsive acceleration magnitude varies as the inverse spacecraft distance from the sun. Indeed, in that case the heliostationary condition is known to be unstable [19] and, therefore, a small error in the orbit insertion (that is, in the sun-spacecraft distance) causes the spacecraft to move away from the desired reference position. The aim of this Note is to study a feedback control system that is able to stabilize the dynamics of a spinning E-sail-based spacecraft around a heliostationary position at a distance of about one astronomical unit from the sun. The analysis is made with a recent mathematical model [20,21], which allows the actual tether shape to be accurately described and the thrust and torque vectors to be written in a compact, analytical, form. In this context, the spacecraft attitude motion is investigated, and the effects of a propulsive torque on the rotational stability are discussed with the aid of a linearized approach.

The Note is organized as follows. The next section extends the results of Ref. [21] by means of closed-form expressions for thrust and torque vectors of a spinning, axisymmetric, E-sail in presence of a small pitch angle (case of near sun-facing E-sail). These equations are then used to analyze the linearized dynamics and control of an E-sail-based spacecraft in a heliostationary position at a sun-spacecraft distance of one astronomical unit. Finally, the last section contains some concluding remarks.

Mathematical Preliminaries

Consider a spacecraft whose primary propulsion system is an E-sail, and assume the vehicle to be modelled as an axially-symmetric body spinning around its symmetry axis. Introduce a principal body reference frame $\mathcal{T}_B(S;\, x_B,\, y_B,\, z_B)$, with unit vectors $\{\hat{\boldsymbol{i}},\, \hat{\boldsymbol{j}},\, \hat{\boldsymbol{k}}\}$, whose origin coincides with the vehicle center-of-mass S, z_B is aligned with the spacecraft symmetry axis, and $(x_B,\, y_B)$ plane coincides with the E-sail nominal plane, see Fig. 1(a).

Using a simplified geometric model to predict the thrust performance [21–23], the E-sail consists of $N > 2$ tethers, uniformly distributed about the z_B-axis. All tethers are maintained at the same electric voltage V, and have the same two-dimensional shape, which is described through a given differentiable function $f = f(x)$, where x is orthogonal to z_B, and $(x,\, z_B)$ defines the plane where the generic tether lies, see Fig. 1(b). The assumption of axial symmetry is consistent with the simulation results obtained for an E-sail shape when its sun-spacecraft line is nearly aligned with the z_B-axis, that is, for a sun-facing E-sail. Note that, according to this simplified model, the tether root belongs to the z_B-axis, whereas in the actual E-sail arrangement all tethers are tied to the outer part of the spacecraft main body [4]. The length L of the generic tether may be written as a function of f as

$$L = \int_0^{x_t} \sqrt{1 + (f')^2}\, \mathrm{d}x \tag{1}$$

where $f' = f'(x) \triangleq \mathrm{d}f/\mathrm{d}x$ is the local tether slope, and x_t is the distance of the tether tip from the spacecraft symmetry axis z_B, see Fig. 1(b).

Thrust and Torque Vector Model

Using the general mathematical model discussed in Ref. [21], both the thrust ($\boldsymbol{F}$) and torque ($\boldsymbol{T}$) vectors acting on an axially-symmetric E-sail of given shape may be expressed in an analytical form as a function of f. In fact, assuming a distance r from the sun of about $r_\oplus \triangleq 1\,\mathrm{au}$, the vectors $\boldsymbol{F}$ and $\boldsymbol{T}$ become [21]

$$\boldsymbol{F} = \frac{1}{2}\, N\, L\, \sigma\, u\, \left[(2-\mathcal{P})\, \hat{\boldsymbol{r}} + (3\,\mathcal{P}-2)\, \left(\hat{\boldsymbol{r}}\cdot\hat{\boldsymbol{k}}\right)\, \hat{\boldsymbol{k}}\right] \tag{2}$$

$$\boldsymbol{T} = \frac{1}{2}\, \mathcal{M}\, N\, L^2\, \sigma\, u\, \left(\hat{\boldsymbol{k}}\times\hat{\boldsymbol{r}}\right) \tag{3}$$

where $\hat{\boldsymbol{r}}$ is the sun-spacecraft unit vector, u is the solar wind speed (with a typical value of about 400 km/s when $r \simeq r_\oplus$), and σ is a design parameter [4, 22, 23] defined as

$$\sigma = \sigma_\oplus\, \left(\frac{r_\oplus}{r}\right) \qquad \text{with} \qquad \sigma_\oplus \triangleq 0.18\, \max(0,\, V - V_w)\, \sqrt{\epsilon_0\, m_p\, n_\oplus} \tag{4}$$

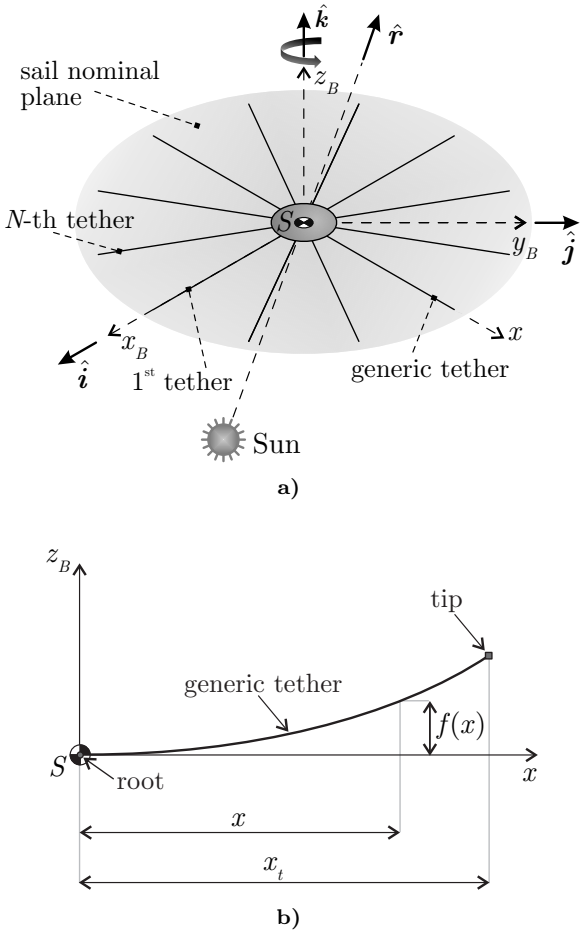

Figure 1 E-sail geometric arrangement. a) Reference frame. b) Generic tether shape. Adapted from Ref. [21].

in which V_w is the electric potential of the solar wind ions (with a typical value of about 1 kV [4]), ϵ_0 is the vacuum permittivity, m_p is the proton mass, and $n_\oplus = 5 \times 10^6\,\mathrm{m}^{-3}$ is the solar wind number density at $r \simeq r_\oplus$. Note that the value of $\sigma_\oplus$ can be varied, within some limits, by changing the tether electric voltage V [4, 22, 23]. For example, assuming $V = 20\,\mathrm{kV}$ [2], the value of the design parameter is $\sigma_\oplus \simeq 9.3 \times 10^{-13}\,\mathrm{kg/m/s}$. In Eqs. (2)-(3), $\mathcal{P} \in [0,\,1]$ and $\mathcal{M} \in [0,\,1]$ are two dimensionless coefficients related to the tether shape f through the equations

$$\mathcal{P} \triangleq \frac{1}{L} \int_0^{x_t} \frac{\mathrm{d}x}{\sqrt{1+(f')^2}} \tag{5}$$

$$\mathcal{M} \triangleq \frac{1}{L^2} \int_0^{x_t} \frac{f\,\left[1+2\,(f')^2\right] + x\,f'}{\sqrt{1+(f')^2}}\,\mathrm{d}x \tag{6}$$

where L is given by Eq. (1).

In the special case of a flat shape, that is, when $\{f,\,f'\} = 0$ and all tethers belong to the same $(x_B,\,y_B)$ plane, Eqs. (1) and (5)-(6) give $L = x_t$, $\mathcal{P} = 1$, and $\mathcal{M} = 0$. In that case, the torque is zero independent of the E-sail attitude, whereas Eq. (2) reduces to [20]

$$\boldsymbol{F} = \frac{1}{2}\,N\,L\,\sigma\,u\,\left[\hat{\boldsymbol{r}} + \left(\hat{\boldsymbol{r}}\cdot\hat{\boldsymbol{k}}\right)\,\hat{\boldsymbol{k}}\right] \tag{7}$$

whose magnitude is

$$\|\boldsymbol{F}\| = \frac{1}{2}\,N\,L\,\sigma\,u\,\sqrt{1+3\,\left(\hat{\boldsymbol{r}}\cdot\hat{\boldsymbol{k}}\right)^2} \tag{8}$$

which depends on the sun-spacecraft distance r through the parameter σ defined in Eq. (4).

Case of Logarithmic Tether Shape

The flat shape may be seen as the first order approximation of the actual shape of a spinning E-sail when its spin axis coincides with the symmetry axis, and the sun-spacecraft line is nearly aligned with the z_B-axis. Actually, each tether inflects due to the interactions with the solar wind, as is confirmed by numerical simulations by Toivanen and Janhunen [23]. In particular, when the E-sail spin rate ω is sufficiently high, that is

$$\omega > \omega_{\min} \qquad \text{with} \qquad \omega_{\min} \triangleq \sqrt{\frac{5\,\sigma\,u}{\rho\,x_t}} \tag{9}$$

where ρ is the tether linear mass density, the equilibrium shape of the generic tether is accurately approximated by a natural logarithmic arc in the form [21]

$$f(x) = b \ln\left(1 + \frac{x}{x_t}\right) \qquad \text{with} \qquad x \in [0,\, x_t] \tag{10}$$

where b is a reference length, defined as

$$b \triangleq \frac{2\,\sigma\,u}{\rho\,\omega^2} \tag{11}$$

However, the spin rate cannot exceed a maximum value $\omega_{\max}$ related to the tether yield strength $\tau_{\max}$, that is [21]

$$\omega < \omega_{\max} \qquad \text{with} \qquad \omega_{\max} \triangleq \sqrt{\frac{2\,\tau_{\max}}{\rho\,x_t^2}} \tag{12}$$

Using a μm-diameter aluminum tether [24] with $\rho \simeq 10^{-5}\,\text{kg/m}$ and $\tau_{\max} = 0.1275\,\text{N}$, the allowable pairs $\{\omega,\, x_t\}$ are shown in Fig. 2 when $x_t \in [1,\, 10]\,\text{km}$. For example, assuming a reference spin rate of $\omega = 10$ revolutions per hour (rph, with $1\,\text{rph} \simeq 1.7453 \times 10^{-3}\,\text{rad/s}$), Fig. 2 shows that the maximum value of x_t is about 9 km. In that case, Fig. 3 shows the variation of $\{L, \mathcal{P}, \mathcal{M}\}$ with $x_t \in [1,\, 9]\,\text{km}$ according to Eqs. (1) and (5)-(6).

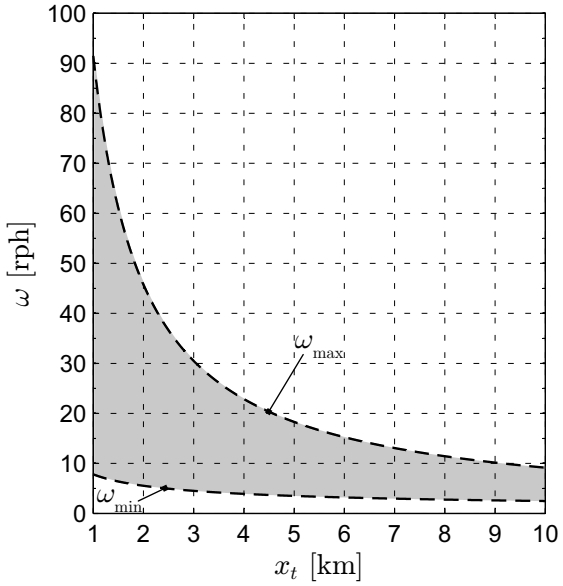

Figure 2 Allowable spin rates as a function of x_t for a μm-diameter aluminum tether [24].

The results of Fig. 3 and, in particular, the function $\mathcal{M} = \mathcal{M}(x_t)$ may also be obtained in an analytical (albeit approximate) form. In fact, the condition $\omega > \omega_{\min}$, with ω taken from Eq. (11) and $\omega_{\min}$ from Eq. (9), implies $b/x_t < 0.4$. Observing that

$$f' = \frac{b}{x_t + x} \leq \frac{b}{x_t} \tag{13}$$

the contribution of $(f')^2$ in Eqs. (1) and (5)-(6) may be neglected, and the result is

$$L \simeq x_t \qquad , \qquad \mathcal{P} \simeq 1 \qquad , \qquad \mathcal{M} \simeq \frac{b\,\ln(2)}{x_t} \tag{14}$$

in accordance with the graphs of Fig. 3. Substituting now Eqs. (14) into Eqs. (2)-(3), the approximate expression of the thrust vector reduces to Eq. (7) (with the magnitude given by Eq. (8)), whereas the torque vector becomes

$$\boldsymbol{T} \simeq \frac{\ln(2)}{2}\, b\, N\, L\, \sigma\, u\, (\hat{\boldsymbol{k}} \times \hat{\boldsymbol{r}}) \tag{15}$$

Equations (7) and (15) are useful for analyzing the perturbed dynamics of an E-sail-based spacecraft in a heliostationary condition, as is discussed in the next section.

Heliostationary E-sail Linearized Dynamics

Consider an E-sail-based spacecraft in a heliostationary position at a distance $r = r_\oplus$ from the sun. In this reference (equilibrium) condition, the spacecraft inertial velocity is zero, the thrust vector direction coincides with the sun-spacecraft line (that is, $\hat{\boldsymbol{k}} \equiv \hat{\boldsymbol{r}}$) and the propulsive acceleration magnitude balances the (local) sun's gravitational acceleration. According to Eqs. (7)-(8) and (15), and bearing in mind Eq. (4), the reference condition is therefore described by

$$\boldsymbol{T} = 0 \qquad , \qquad \frac{\|\boldsymbol{F}\|}{m} = \frac{N\,L\,\sigma_\oplus\,u}{m} \equiv \frac{\mu_\odot}{r_\oplus^2} \tag{16}$$

where m is the (constant) total spacecraft mass, and $\mu_\odot$ is the sun's gravitational parameter.

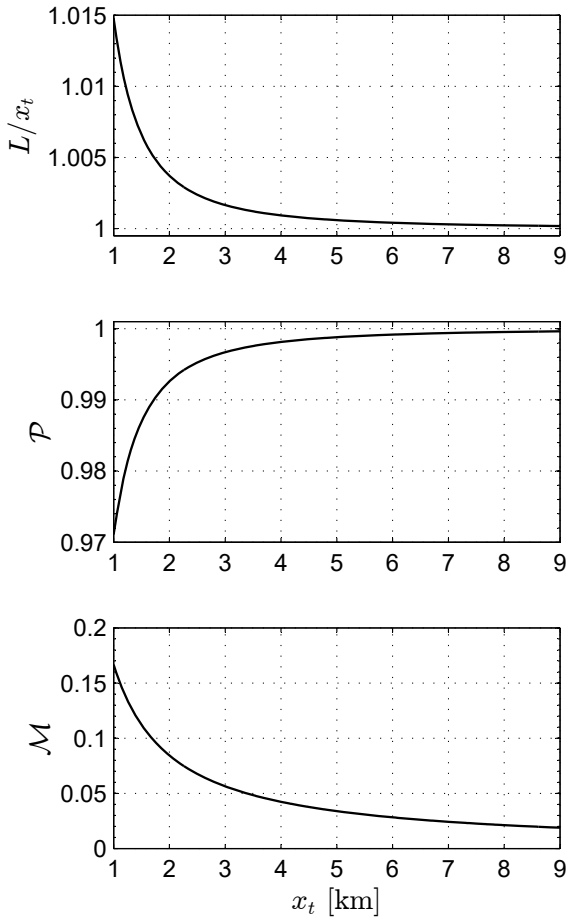

Figure 3 Variation of $\{L, \mathcal{P}, \mathcal{M}\}$ with x_t when $\omega = 10\,\mathrm{rph}$.

Spacecraft Position Stability and Control

According to Ref. [19], the heliostationary condition is unstable. In fact, from Eqs. (4), (8) and (16), the propulsive acceleration in the neighbourhood of the reference position is

$$\frac{\|\boldsymbol{F}\|}{m} = \frac{N\,L\,\sigma_\oplus\,u}{m}\,\left(\frac{r_\oplus}{r}\right) = \frac{\mu_\odot}{r_\oplus^2}\,\left(\frac{r_\oplus}{r}\right) \tag{17}$$

and the spacecraft equation of motion is therefore

$$\ddot{r} = -\frac{\mu_\odot}{r^2} + \frac{\|\boldsymbol{F}\|}{m} = \frac{\mu_\odot}{r_\oplus^2}\,\left[\frac{r_\oplus}{r} - \left(\frac{r_\oplus}{r}\right)^2\right] \tag{18}$$

whose linearization gives [19]

$$\ddot{\nu} - \frac{\mu_\odot}{r_\oplus^3}\,\nu = 0 \tag{19}$$

where $\nu \triangleq (r/r_\oplus - 1)$ is the dimensionless error in radial (i.e., sun-spacecraft) distance. Accordingly, a control system must be implemented to make the heliostationary condition stable. A simple solution is to change the tether electric voltage V (and so, the value of $\sigma_\oplus$) as a function of the sun-spacecraft distance. The voltage is therefore conveniently adjusted so as to induce a variation of the propulsive acceleration in the form of a proportional control law, that is

$$\frac{\|\boldsymbol{F}\|}{m} = \frac{\mu_\odot}{r_\oplus^2}\,\left(\frac{r_\oplus}{r}\right)\,(1 - k_p\,\nu) \tag{20}$$

where k_p is a constant dimensionless parameter. Since the propulsive acceleration magnitude $\|\boldsymbol{F}\|/m$ is proportional to the tether voltage V, see Eqs. (4) and (8), the maximum percentage variation of V is

$$\frac{\Delta V_{\max}}{\overline{V}} = k_p\,(\nu_{\max} - \nu_{\min}) \tag{21}$$

where $\nu_{\max}$ (or $\nu_{\min}$) is the maximum (or minimum) value of ν, while $\overline{V}$ is the nominal value of the tether voltage. Substituting Eq. (20) into (18), the linearized spacecraft dynamics in the neighbourhood of the reference position becomes

$$\ddot{\nu} + \frac{\mu_\odot}{r_\oplus^3}\,(k_p - 1)\,\nu = 0 \tag{22}$$

which describes a harmonic motion when $k_p > 1$, that is

$$\nu(t) = \nu_0 \, \cos(\omega_n \, t) + \frac{\dot{\nu}_0}{\omega_n} \, \sin(\omega_n \, t) \tag{23}$$

where $\omega_n \triangleq \sqrt{\mu_\odot \, (k_p - 1)/r_\oplus^3}$ is the natural frequency, and $\{\nu_0, \, \dot{\nu}_0\}$ are the initial conditions. Note that the oscillation period, given by $2\pi/\omega_n$, is less (greater) than 1 year if $k_p > 2$ ($1 < k_p < 2$), while $\omega_n = \sqrt{\mu_\odot / r_\oplus^3}$ when $k_p = 2$. In the special case when $\dot{\nu}_0 = 0$, Eqs. (21) and (23) give $\Delta V_{\max}/\overline{V} = 2 \, k_p \, \nu_0$, that is, the maximum percentage variation of the tether voltage is proportional (through k_p) to the orbit insertion radial error ν_0. Although the linearized dynamics (22) has imaginary poles and so no conclusion can be inferred on the stability of the nonlinear model, the latter may be shown to be locally stable around the equilibrium condition $\nu(0) = 0$ and $\dot{\nu}(0) = 0$, as is discussed in the Appendix.

The radial oscillations described by Eq. (23) can be damped out with a proportional-derivative control system. In that case the tether voltage is modulated in such a way that the propulsive acceleration is in the form

$$\frac{\|\boldsymbol{F}\|}{m} = \frac{\mu_\odot}{r_\oplus^2} \, \left(\frac{r_\oplus}{r}\right) \, \left(1 - k_p \, \nu - \frac{k_d \, \dot{\nu}}{\sqrt{\mu_\odot / r_\oplus^3}} \right) \tag{24}$$

where $k_d > 0$ is a constant dimensionless parameter. The linearized spacecraft dynamics are

$$\ddot{\nu} + \frac{\mu_\odot}{r_\oplus^3} \, \left[(k_p - 1) \, \nu + \frac{k_d \, \dot{\nu}}{\sqrt{\mu_\odot / r_\oplus^3}} \right] = 0 \tag{25}$$

which describes a second-order system with damping factor $\zeta \triangleq k_d / \left(2 \sqrt{k_p - 1} \right)$ and natural frequency ω_n. Note that, when $k_d = 2 \sqrt{k_p - 1}$ (that is, $\zeta = 1$), the time variation of the radial error is

$$\nu(t) = \exp\left(-\omega_n \, t\right) \, \left[\nu_0 + \left(\dot{\nu}_0 + \omega_n \, \nu_0 \right) \, t \right] \tag{26}$$

and the maximum variation of tether voltage is $\Delta V_{\max}/\overline{V} = \nu_0$ if $\dot{\nu}_0 = 0$.

Attitude Dynamics

When the spacecraft attitude is perturbed from its reference condition, that is, when the z_B-axis slightly differs from the sun-spacecraft direction ($\hat{\boldsymbol{k}} \neq \hat{\boldsymbol{r}}$), the spacecraft experiences a non-zero propulsive torque whose approximate expression is given by Eq. (15). The components of $\boldsymbol{T}$ in the body reference frame can be written as a function of three classical Euler's angles $\{\phi, \, \theta, \, \psi\}$, which define the orientation of $\mathcal{T}_B$ with respect to an inertial reference frame $\mathcal{T}_I(S; \, x_I, \, y_I, \, z_I)$ of unit vectors $\{\hat{\boldsymbol{i}}_I, \, \hat{\boldsymbol{j}}_I, \, \hat{\boldsymbol{k}}_I\}$, where $\hat{\boldsymbol{k}}_I \equiv \hat{\boldsymbol{r}}$, and $\hat{\boldsymbol{i}}_I$ points towards a fixed direction in space. Using a rotational sequence [25] $3(\psi) \rightarrow 1(\phi) \rightarrow 2(\theta)$ to describe the orientation of $\mathcal{T}_B$ relative to $\mathcal{T}_I$, the components of $\hat{\boldsymbol{r}}$ in the body reference frame are

$$[\hat{\boldsymbol{r}}]_{\mathcal{T}_B} = \begin{bmatrix} -\cos\phi \, \sin\theta \\ \sin\phi \\ \cos\phi \, \cos\theta \end{bmatrix} \tag{27}$$

The sail attitude may also be expressed using the pitch angle $\alpha_n \in [0, \, \pi]$ and clock angle $\delta_n \in [0, \, 2\pi]$, defined as

$$\alpha_n = \arccos(\hat{\boldsymbol{r}} \cdot \hat{\boldsymbol{k}}) \quad , \quad \delta_n = \begin{cases} \arccos\left(\dfrac{\hat{\boldsymbol{r}} \cdot \hat{\boldsymbol{i}}}{||\hat{\boldsymbol{r}} \times \hat{\boldsymbol{k}}||} \right) & \text{if } (\hat{\boldsymbol{r}} \cdot \hat{\boldsymbol{j}}) \geq 0 \\ 2\pi - \arccos\left(\dfrac{\hat{\boldsymbol{r}} \cdot \hat{\boldsymbol{i}}}{||\hat{\boldsymbol{r}} \times \hat{\boldsymbol{k}}||} \right) & \text{if } (\hat{\boldsymbol{r}} \cdot \hat{\boldsymbol{j}}) < 0 \end{cases} \tag{28}$$

that are related to the Euler's angles through the equations

$$\cos\alpha_n = \cos\phi \, \cos\theta \quad , \quad \sin\delta_n = \frac{\sin\phi}{\sin\alpha_n} \quad , \quad \cos\delta_n = -\frac{\cos\phi \, \sin\theta}{\cos\alpha_n} \tag{29}$$

Assuming α_n to be sufficiently small in the perturbed condition, which implies $\{\phi, \, \theta\} \ll 1$ (recall that $\theta = \phi = 0$ in the reference condition), Eq. (27) reduces to

$$[\hat{\boldsymbol{r}}]_{\mathcal{T}_B} \simeq \begin{bmatrix} -\theta \\ \phi \\ 1 \end{bmatrix} \tag{30}$$

and the linearized kinematic equations are [26]

$$\dot{\phi} = \Omega_x + \theta \, \omega \tag{31}$$

$$\dot{\theta} = \Omega_y - \phi \, \left(\omega - \theta \, \Omega_x \right) \tag{32}$$

$$\dot{\psi} = \omega - \theta \, \Omega_x \tag{33}$$

where $[\Omega_x,\, \Omega_y,\, \omega]^{\mathrm{T}} = [\boldsymbol{\Omega}]_{\mathcal{T}_B}$ are the components in $\mathcal{T}_B$ of the spacecraft angular velocity vector $\boldsymbol{\Omega}$. The kinematic equations can be further simplified by observing that $\omega \gg \theta\,\Omega_x$, from which

$$\dot{\phi} = \Omega_x + \theta\,\omega \tag{34}$$

$$\dot{\theta} = \Omega_y - \phi\,\omega \tag{35}$$

$$\dot{\psi} = \omega \tag{36}$$

Bearing in mind Eq. (15) and using Eq. (30), the components of the propulsive torque vector in $\mathcal{T}_B$ become

$$[\boldsymbol{T}]_{\mathcal{T}_B} = -\frac{\ln(2)}{2}\, b\, N\, L\, \sigma\, u \begin{bmatrix} \phi \\ \theta \\ 0 \end{bmatrix} \tag{37}$$

Accordingly, the Euler's equations for the axially-symmetric E-sail are given by

$$\dot{\Omega}_x = -h\,\omega^2\,\phi + \lambda\,\omega\,\Omega_y \tag{38}$$

$$\dot{\Omega}_y = -h\,\omega^2\,\theta - \lambda\,\omega\,\Omega_x \tag{39}$$

$$\dot{\omega} = 0 \tag{40}$$

where

$$\lambda \triangleq \frac{I_t - I_z}{I_t} \qquad , \qquad h \triangleq \frac{\ln(2)\, b\, N\, L\, \sigma\, u\, (1-\lambda)}{2\, I_z\, \omega^2} \tag{41}$$

in which I_z and I_t are the longitudinal and transverse moments of inertia, respectively.

Note that h is a dimensionless parameter depending on the tether shape through the reference distance b, and on the sun-spacecraft distance r (or tether voltage V) through the design parameter σ. Recalling the perturbed motion of the spacecraft center-of-mass around the reference position described by Eq. (18), the dimensionless parameter h is a function of time through σ. However, the value of σ changes with time very slowly when compared to the rotational period (since $\omega_n \ll \omega$), so that h can be considered as a constant parameter in the analysis of the E-sail attitude dynamics. From Eqs. (36) and (40), the spin rate ω is a constant or motion, and $\psi = \omega\, t + \psi_0$, where ψ_0 is the initial value of ψ. Using the dimensionless time $\tilde{t}$ and the angular velocities $\{\widetilde{\Omega}_x,\, \widetilde{\Omega}_y\}$ defined as

$$\tilde{t} \triangleq t\,\omega \quad , \quad \widetilde{\Omega}_x \triangleq \frac{\Omega_x}{\omega} \quad , \quad \widetilde{\Omega}_y \triangleq \frac{\Omega_y}{\omega} \tag{42}$$

Eqs. (34)-(35) and (38)-(39) may be equivalently written in matrix form as

$$\frac{\mathrm{d}\boldsymbol{x}}{\mathrm{d}\tilde{t}} = \mathbb{A}\,\boldsymbol{x} \qquad \text{with} \qquad \mathbb{A} \triangleq \begin{bmatrix} 0 & \lambda & -h & 0 \\ -\lambda & 0 & 0 & -h \\ 1 & 0 & 0 & 1 \\ 0 & 1 & -1 & 0 \end{bmatrix} \tag{43}$$

where $\boldsymbol{x} \triangleq [\widetilde{\Omega}_x,\, \widetilde{\Omega}_y,\, \phi,\, \theta]^{\mathrm{T}}$ is the dimensionless state vector. Using the Routh-Hurwitz stability criterion, and taking into account that $h > 0$ and $\lambda < 0$, it may be verified that the linear differential system of Eq. (43) is stable and is characterized by a pair of imaginary poles. Therefore, the presence of a propulsive torque vector, due to a pitch angle α_n different from zero, does not affect the (natural) stability of the E-sail rotational motion.

The stability of the nonlinear E-sail attitude dynamics has been investigated by extensive simulations. For exemplary purposes, consider the case of initial conditions

$$\{\alpha_{n_0},\, \delta_{n_0}\} = \{5,\, 90\}\ \mathrm{deg} \quad , \quad \{\Omega_{x_0},\, \Omega_{y_0},\, \omega_0\} = \{0,\, 0,\, 40\}\ \mathrm{rph} \tag{44}$$

and use the same design parameters (ρ and σ) as those discussed in the previous section with $N = 500$, $L = 2\,\mathrm{km}$, $I_t = 1000\,\mathrm{kg\,m^2}$, and $\lambda = -1/2$. An initial spin rate equal to 40 rph implies $\mathcal{M} \simeq 0.0026$ and $\mathcal{P} \simeq 1$ (note that, when $L = 2\,\mathrm{km}$, the spacecraft spin rate must range within the interval $[5.63,\, 45.74]$ rph). The simulation results are reported in Fig. 4. The pitch angle shows a periodic time variation due to a nutation motion of the spacecraft symmetry axis. The maximum value of α_n coincides with α_{n_0}, while its oscillation period is equal to 46 s. Let k_x, k_y and k_z be the components of $\hat{\boldsymbol{k}}$ in the frame $\mathcal{T}_I$. Figure 4 illustrates the time variations of k_x and k_y, and shows the combined effect of a nutation and a precession motion, the latter having a period of about 6.5 minutes.

The long-term propulsive effect due the torque acting on the spacecraft is better appreciated by simulating the thrust components in the inertial frame. This is possible using the following equations

$$F_x = \frac{N\, L\, \sigma\, u}{2}\ (3\,P - 2)\ [\cos\phi\, \cos\theta\, (\sin\theta\, \cos\psi + \sin\phi\, \cos\theta\, \sin\psi)] \tag{45}$$

$$F_y = \frac{N\, L\, \sigma\, u}{2}\ (3\,P - 2)\ [\cos\phi\, \cos\theta\, (\sin\theta\, \sin\psi - \sin\phi\, \cos\theta\, \cos\psi)] \tag{46}$$

$$F_z = \frac{N\, L\, \sigma\, u}{2}\ \left[2 - P + (3\,P - 2)\, \cos^2\phi\, \cos^2\theta\right] \tag{47}$$

where F_x, F_y and F_z are the components of $\boldsymbol{F}$ in $\mathcal{T}_I$. Figure 5 shows the simulation results. The thrust components on the plane $(x_I,\, y_I)$ are characterized by a zero mean value, while the radial component has a short period oscillation with a small amplitude, due to the nutation motion.

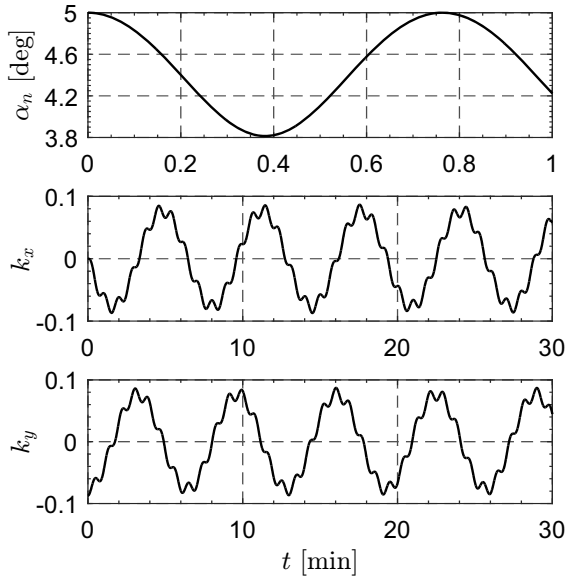

Figure 4 Time variation of α_n, k_x, and k_y.

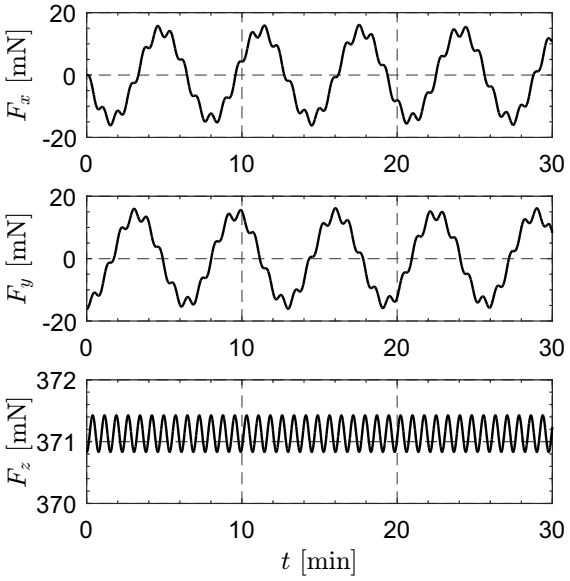

Figure 5 Time variation of the components of $\boldsymbol{F}$.

Conclusions

The dynamics of a spinning E-sail-based-spacecraft exhibits a marked separation between attitude and orbital motion. In particular, with a suitable modulation of the tether electric voltage, the spacecraft center-of-mass moves along the sun-spacecraft line around its nominal heliostationary position. When a simple proportional controller is used, the maximum variation in tether voltage is proportional to the (radial) distance error in orbit insertion. The resulting spacecraft motion is an undamped harmonic oscillation with a period on the order of some years. The combined effect of tether inflection and deviation from the sun-facing condition (that is, the presence of a small pitch angle) generates a propulsive torque that induces an undamped oscillatory motion with a frequency comparable to the spacecraft spin rate. Despite the propulsive torque due to the perturbation in pitch angle, the attitude motion is stable and can be conveniently studied using a linearized model and a constant state matrix.

The proposed approach can be extended to the case of an E-sail-based spacecraft in a non-Keplerian circular (or nearly circular) orbit, with a radius on the order of one astronomical unit. In that case, the thrust vector is required to be aligned with the sun-spacecraft direction, whereas the propulsive acceleration magnitude is a (small) fraction of the local sun's gravitational acceleration. The orbital motion, however, induces a time increase of the pitch angle, since the spin axis points a fixed direction in the space. A suitable control system is therefore necessary to re-align the spin axis along the sun-spacecraft line.

Appendix

With reference to Eqs. (18) and (20), the nonlinear radial dynamics of an E-sail with proportional control around a heliostationary equilibrium position at a distance $r = r_\oplus$ from the sun, is

$$\ddot{\nu} = \frac{\mu_\odot}{r_\oplus^3} \frac{(1-k_p)\,\nu - k_p\,\nu^2}{(1+\nu)^2} \tag{48}$$

Let $\boldsymbol{q} = [q_1, q_2]^{\mathrm{T}}$, with $q_1 \triangleq \nu$ and $q_2 \triangleq \dot{\nu}$, then Eq. (48) can be rewritten as

$$\begin{cases} \dot{q}_1 = q_2 \\ \dot{q}_2 = \dfrac{\mu_\odot}{r_\oplus^3} \dfrac{(1-k_p)\,q_1 - k_p\,q_1^2}{(1+q_1)^2} \triangleq g(q_1) \end{cases} \tag{49}$$

Introduce the candidate Lyapunov function

$$\mathscr{V}(\boldsymbol{q}) = -\int g(q_1)\,\mathrm{d}q_1 + \frac{1}{2}\,q_2^2 \tag{50}$$

with $\mathscr{V}(\boldsymbol{0}) = 0$, from which

$$\mathscr{V}(\boldsymbol{q}) = \frac{\mu_\odot}{r_\oplus^3} \left[\frac{q_1}{1+q_1} + k_p\,q_1 - (1+k_p)\,\ln(1+q_1)\right] + \frac{1}{2}\,q_2^2 \tag{51}$$

It may be verified that, when $k_p > 1$, $\mathscr{V}(\boldsymbol{q}) > 0\ \forall \boldsymbol{q} \neq \boldsymbol{0}$ and $\dot{\mathscr{V}}(\boldsymbol{q}) = 0\ \forall \boldsymbol{q}$. This implies that $\mathscr{V}(\boldsymbol{q})$ is actually a Lyapunov function and the origin is a locally stable point when a proportional feedback control law is adopted.

References

[1] Janhunen, P., "Electric Sail for Spacecraft Propulsion," *Journal of Propulsion and Power*, Vol. 20, No. 4, July-August 2004, pp. 763–764. doi: 10.2514/1.8580.

[2] Mengali, G., Quarta, A. A., and Janhunen, P., "Electric Sail Performance Analysis," *Journal of Spacecraft and Rockets*, Vol. 45, No. 1, January-February 2008, pp. 122–129. doi: 10.2514/1.31769.

[3] Janhunen, P. and Sandroos, A., "Simulation study of solar wind push on a charged wire: basis of solar wind electric sail propulsion," *Annales Geophysicae*, Vol. 25, No. 3, March 2007, pp. 755–767. doi: 10.5194/angeo-25-755-2007.

[4] Janhunen, P., Toivanen, P. K., Polkko, J., et al., "Invited article: Electric solar wind sail: Toward test missions," *Review of Scientific Instruments*, Vol. 81, No. 11, November 2010, pp. 111301–1–11301–11. doi: 10.1063/1.3514548.

[5] Janhunen, P., Quarta, A. A., and Mengali, G., "Electric solar wind sail mass budget model," *Geoscientific Instrumentation, Methods and Data Systems*, Vol. 2, No. 1, 2013, pp. 85–95. doi: 10.5194/gi-2-85-2013.

[6] Forward, R. L., "Statite - A spacecraft that does not orbit," *Journal of Spacecraft and Rockets*, Vol. 28, No. 5, Septemper 1991, pp. 606–611. doi: 10.2514/3.26287.

[7] Baig, S. and McInnes, C. R., "Light-Levitated Geostationary Cylindrical Orbits are Feasible," *Journal of Guidance, Control, and Dynamics*, Vol. 33, No. 3, May-June 2010, pp. 782–793. doi: 10.2514/1.46681.

[8] McKay, R. J., Macdonald, M., Biggs, J. D., and McInnes, C. R., "Survey of Highly-Non-Keplerian Orbits with Low-Thrust Propulsion," *Journal of Guidance, Control, and Dynamics*, Vol. 34, No. 3, May-June 2011, pp. 645–666. doi: 10.2514/1.52133.

[9] Zeng, X., Alfriend, K. T., and Vadali, S. R., "Solar sail planar multireversal periodic orbits," *Journal of Guidance, Control, and Dynamics*, Vol. 37, No. 2, February 2014, pp. 674–681. doi: 10.2514/1.58598.

[10] McInnes, C. R., "Artificial Lagrange Points for a Partially Reflecting Flat Solar Sail," *Journal of Guidance, Control, and Dynamics*, Vol. 22, No. 1, January-February 1999, pp. 185–187. doi: 10.2514/2.7627.

[11] Aliasi, G., Mengali, G., and Quarta, A. A., "Artificial Lagrange Points for Solar Sail with Electrochromic Material Panels," *Journal of Guidance, Control, and Dynamics*, Vol. 36, No. 5, September-October 2013, pp. 1544–1550. doi: 10.2514/1.58167.

[12] McInnes, C. R., "Inverse solar sail trajectory problem," *Journal of Guidance, Control, and Dynamics*, Vol. 26, No. 2, March-April 2003, pp. 369–371. doi: 10.2514/2.5057.

[13] Dandouras, I., Pirard, B., and Prado, J. Y., "High Performance Solar Sails for Linear Trajectories and Heliostationary Missions," *Advances in Space Research*, Vol. 34, No. 1, 2004, pp. 198–203. doi: 10.1016/j.asr.2003.02.055.

[14] Mengali, G. and Quarta, A. A., "Optimal heliostationary missions of high-performance sailcraft," *Acta Astronautica*, Vol. 60, No. 8-9, April-May 2007, pp. 676–683. doi: 10.1016/j.actaastro.2006.07.018.

[15] Quarta, A. A. and Mengali, G., "Solar Sail Capabilities to Reach Elliptic Rectilinear Orbits," *Journal of Guidance, Control, and Dynamics*, Vol. 34, No. 3, May-June 2011, pp. 923–926. doi: 10.2514/1.51638.

[16] Quarta, A. A. and Mengali, G., "Optimal Solar Sail Transfer to Linear Trajectories," *Acta Astronautica*, Vol. 82, No. 2, February 2013, pp. 189–196. doi: 10.1016/j.actaastro.2012.03.005.

[17] Fu, B., Sperber, E., and Eke, F., "Solar sail technology–A state of the art review," *Progress in Aerospace Sciences*, Vol. 86, October 2016, pp. 1–19. doi: 10.1016/j.paerosci.2016.07.001.

[18] Montgomery, E. E., Garbe, G. P., and Heaton, A. F., "Places Only Solar Sails Can Go," *AIAA/ICAS International Air and Space Symposium and Exposition: The Next 100 Years*, Dayton, Ohio, July 14–17 2003, doi: 10.2514/6.2003-2836.

[19] Niccolai, L., Quarta, A. A., and Mengali, G., "Electric sail-based displaced orbits with refined thrust model," *Proceedings of the Institution of Mechanical Engineers, Part G: Journal of Aerospace Engineering*, Vol. 232, No. 3, March 2018, pp. 423–432. doi: 10.1177/0954410016679195.

[20] Huo, M., Mengali, G., and Quarta, A. A., "Electric Sail Thrust Model from a Geometrical Perspective," *Journal of Guidance, Control and Dynamics* , Vol. 41, No. 3, March 2018, pp. 735–741. doi: 10.2514/1.G003169.

[21] Bassetto, M., Mengali, G., and Quarta, A. A., "Thrust and Torque Vector Characteristics of Axially-symmetric E-Sail," *Acta Astronautica*, Vol. 146, May 2018, pp. 134–143. doi: 10.1016/j.actaastro.2018.02.035.

[22] Toivanen, P. and Janhunen, P., "Spin Plane Control and Thrust Vectoring of Electric Solar Wind Sail," *Journal of Propulsion and Power*, Vol. 29, No. 1, January-February 2013, pp. 178–185. doi: 10.2514/1.B34330.

[23] Toivanen, P. and Janhunen, P., "Thrust vectoring of an electric solar wind sail with a realistic sail shape," *Acta Astronautica*, Vol. 131, 2017, pp. 145–151. doi: 10.1016/j.actaastro.2016.11.027.

[24] Seppänen, H., Rauhala, T., Kiprich, S., Ukkonen, J., Simonsson, M., Kurppa, R., Janhunen, P., and Hæggstrom, E., "One kilometer (1 km) electric solar wind sail tether produced automatically," *Review of Scientific Instruments*, Vol. 84, No. 9, September 2013. doi: 10.1063/1.4819795.

[25] Wertz, J. R., editor, *Spacecraft Attitude Determination and Control*, Astrophysics and Space Science Library, Springer Netherlands, Dordrecht, Holland, 1st ed., 1978, pp. 760–766, doi: 10.1007/978-94-009-9907-7.

[26] Longuski, J. M., Gick, R. A., Ayoubi, M. A., and Randall, L. A., "Analytical Solutions for Thrusting, Spinning Spacecraft Subject to Constant Forces," *Journal of Guidance, Control, and Dynamics*, Vol. 28, No. 6, November 2005, pp. 1301–1308. doi: 10.2514/1.12272.